Estuarine, Coastal and Shelf Science 95 (2011) 119–134

Contents lists available at SciVerse ScienceDirect

Estuarine, Coastal and Shelf Science

journal homepage: www.elsevier.com/locate/ecss

# Applicability of sediment transport models to evaluate medium term evolution of tidal inlet systems

A. Pacheco[a,*], J.J. Williams[b], Ó. Ferreira[a], E. Garel[a], S. Reynolds[c]

[a] CIMA/Universidade do Algarve, Edifício 7, Campus de Gambelas, Faro 8005-139, Portugal
[b] ABP Marine Environmental Research Ltd, Suite B, Waterside House, Town Quay, Southampton SO14 2AQ, UK
[c] University of Plymouth, School of Marine Science and Engineering, Plymouth PL4 8AA, UK

ARTICLE INFO

*Article history:*
Received 11 August 2010
Accepted 20 August 2011
Available online 26 August 2011

*Keywords:*
tidal inlets
barrier islands
tidal currents
coastal morphology
sediment transport

ABSTRACT

This paper derives local formulae to estimate bed roughness and suspended transport and present a method to calculate net sediment transport at tidal inlet systems, combining field data and a range of well established empirical formulations. To accomplish this, measurements spanning a spring-tidal cycle of mean water levels, waves, near-bed flow turbulence and bed forms were obtained from the Ancão Inlet, Ria Formosa lagoon system, Portugal. High-resolution hydrodynamic data were gathered using acoustic equipments and by measuring sediment properties (grain-size diameter and bed form dimensions) under fair-weather conditions. The results compared favourably with available direct and indirect field observations of sediment transport rates. The approach appears to be robust and widely applicable and so can be applied to the same conditions in any tidal inlet system. This is of particular importance when attempting to understand sediment transport at inlet mouths, and has practical applications in a range of coastal engineering and coastal management areas concerned with navigation safety, coastal erosion, ecosystem health and water quality. The study discusses the applicability of the method on evaluating system flushing capacity, giving important insights on multiple inlet evolution, particularly with regard to their persistence through time. The methodological framework can be applied to assess the long-term stability of single- and multiple-inlet systems, provided that estimates of sediment storage at ebb-tidal deltas are available and sediment transport estimates during storm events are statistically considered.



## 1. Introduction

Tidal inlets are dynamic coastal features that play an important role in navigation, sediment supply to adjacent beaches and nutrient exchanges between backbarrier systems and the coastal zone (FitzGerald, 1996). Several authors have proposed conceptual or semi-empirical models that explain tidal inlet function and morphological evolution in terms of wave or tidal flow dominance (e.g. Oertel, 1972; Hayes, 1979; FitzGerald, 1996; FitzGerald et al., 2001; Morris et al., 2001, 2004). Other approaches advocate the use of qualitative conceptual models that are based on the historical evolution of inlet morphology (e.g. channel, ebb/flood shoals) and provide regional perspectives on interactions between beach processes and offshore areas (e.g. Kana and Stevens, 1992; Kana et al., 1999; Rosati and Kraus, 1999; Rosati, 2005; Elias and van der Spek, 2006; Pacheco et al., 2008). Despite progress in this area, no model is yet able to predict quantitatively the evolution of inlet morphology in the medium- to long-term and thus the need to consider inlet evolution in conceptual terms remains.

Quantification of sediment transport in tidal inlets is a fundamental requirement to support both conceptual and numerical modelling of tidal inlet function and evolution. Since field-based studies of sediment transport have the potential to quantify the magnitude and direction of net sediment transport, they may assist in identifying evolutionary trends for a single tidal inlet or a multi-inlet system. However, obtaining high-resolution data of sediment transport on real field conditions is a difficult task. The use of empirical relationships between fluid flow and an erodible sediment bed enables the estimation of sediment transport over a range of prescribed bed form and flow parameters (Nielsen, 1992; Soulsby, 1997; van Rijn, 2007a,b) and shown to work well (van Rijn, 2007a,b).

Here we present a method to estimate net sediment transport rates, using the Ria Formosa lagoon system of Southern Portugal as

* Corresponding author.
*E-mail addresses:* ampacheco@ualg.pt (A. Pacheco), oferreir@ualg.pt (Ó. Ferreira), egarel@ualg.pt (E. Garel), saul.reynolds@plymouth.ac.uk (S. Reynolds).

0272-7714/$ – see front matter © 2011 Elsevier Ltd. All rights reserved.
doi:10.1016/j.ecss.2011.08.027

a case-study. The method combines field data with a range of well established semi-empirical formulae. These data include: a) high-frequency flow and water level data obtained at one inlet of the area (the Ancão Inlet); and b) boat-mounted Acoustic Doppler Current Profiler (ADCP) data obtained for complete tidal cycles (*c.* 12.5 h) in the 5 other tidal inlets of the Ria Formosa during spring- and neap tide conditions. The focus of the study is current-generated sediment transport under fair-weather conditions. The Ancão Inlet was chosen as a case-study due to the existence and availability of datasets collected during and after the INDIA Project (European Union Project, MAST3-CT97-0106). The applicability of the presented method on estimating net sediment transport is discussed and was motivated to assess the flushing capability of tidal inlet systems during neap/spring-tide conditions.

## 2. Field site description

The Ria Formosa is a multi-inlet barrier island system located in Southern Portugal (Fig. 1). It comprises five islands and two peninsulas separated by six tidal inlets: two relocated inlets (Ancão and Fuseta), two artificially opened and stabilised inlets (Faro-Olhão and Tavira) and two natural inlets (Armona and Lacém). The embayment is characterised by large salt marshes, sand flats and a complex network of natural and partially dredged channels.

Tides in the area are semi-diurnal with typical average ranges of 2.8 m for spring-tides and 1.3 m for neap tides. A maximum tidal range of 3.5 m occurs during equinoctial tides. Harmonic analysis revealed $M_2$ as the dominant component with tides inside the lagoon being strongly distorted (Salles et al., 2005). Wave climate in the area is moderate to high (offshore annual mean significant wave height $H_s \sim 1$ m and peak period $T_p$ of 8.2 s, with storms characterised by $H_s > 3$ m). Approximately 71% of waves are from the W–SW, with ~23% coming from the E–SE (Costa et al., 2001). Available data from the Faro wave buoy show that ~70% of the waves are in the range of 0–1 m and with directions from W to SW (Costa et al., 2001). Longshore currents in the area typically flow from W to E. Estimates of net annual longshore sediment transport obtained by various authors range between $6.0 \times 10^4$ to $3.0 \times 10^5$ m$^3$ year$^{-1}$ (Concejo et al., 2006).

## 3. Methods

In order to provide suitable data for computation of bed load and suspended sediment transport, high-frequency measurements of flow turbulence were obtained in the Ancão Inlet close to the spring low-water line in October 2007 using an Acoustic Doppler Velocimeter-ADV (SonTek/YSI 10 MHz Ocean Probe) with an internal Pressure Transducer, PT (Fig. 1). The ADV collected data at 25 Hz and operated in continuous burst mode (burst interval 1800 s and 30,000 samples per burst) and for one complete tidal cycle. In addition, two *in situ* Level Troll 300 PTs were deployed on the seaward and lagoon sides of the Ancão Inlet to measure the difference in water level (pressure sensor accuracy of ±0.2% and resolution of 0.005%, for full-scale operation). Measurements were obtained for $H_s < 0.25$ m and wave set up effects were very small. The PT in the lagoon was located very close to the inlet and thus not affected by water slopes in the backbarrier channel. These instruments were also located close to the spring low-water line and surveyed using a Real Time Kinematic Differential Global Positioning System (RTK-DGPS) to determine their vertical and horizontal coordinates (±5 mm). PT internal clocks were synchronised and pressure data were recorded at 1 Hz. Pressure values were adjusted to account for local barometric pressure and corrected for depth attenuation of the wave-induced pressure signal (Bishop and Donelan, 1987). Measurements of vertical current velocity profiles were obtained across each inlet cross-section of the Ria Formosa inlets, using a boat-mounted ADCP (SonTek/YSI 1500 kHz) with bottom tracking, every hour during ~12.5 h spring and neap tidal cycles. Samples of bottom surficial sediment were also collected across each tidal inlet cross-section (three samples at five spatial locations equally spaced along the inlet cross-section) with a small grab sampler. In all cases measurements were undertaken during

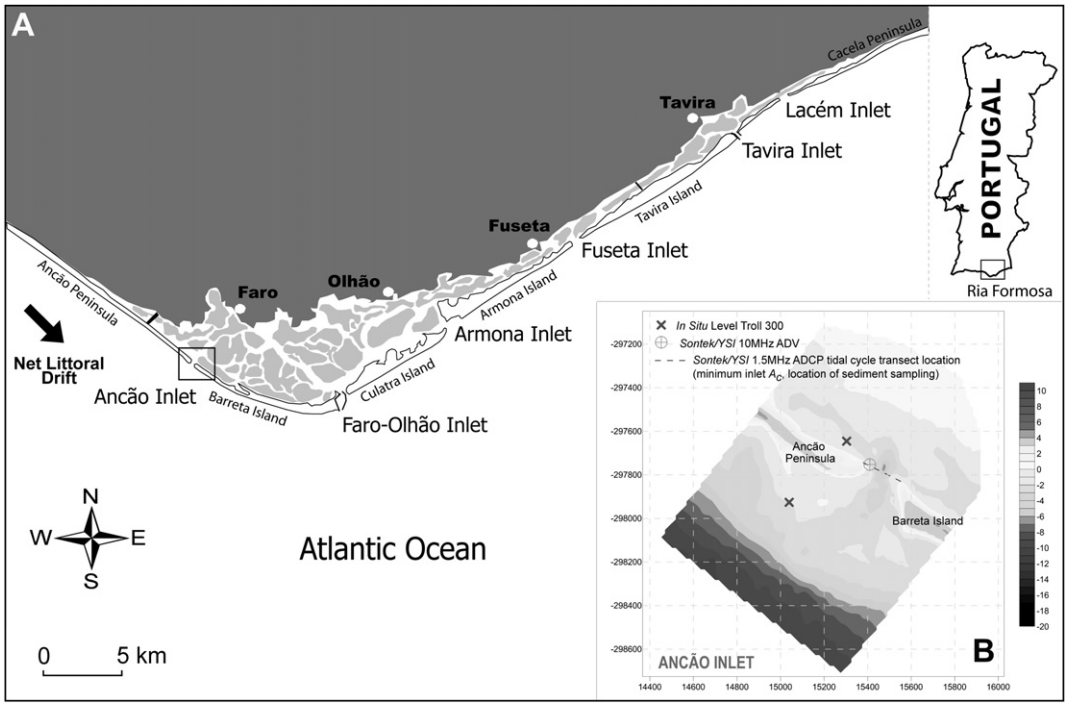


**Fig. 1.** Ria Formosa Multi-Inlet System (Southern Portugal) showing the Ancão Inlet and the location of the deployed equipment.

low hydrodynamic conditions prevailing in this area (fair-weather, W–SW wave conditions) (see Pacheco et al. (2010) for further details).

### 3.1. Bed sediment properties

Organic matter was removed from the sediment samples using hydrogen peroxide and samples were weighed, washed and oven-dried before being sieved at ½ ø intervals. Required grain-size parameters were computed according to the methodology described by Folk and Ward (1957) using the computer program Gradistat (Blott and Pye, 2001). Carbonate percentages were measured in ø intervals by weight loss on the addition of 10% HCl to dissolve shell fragments. Average grain diameters were then calculated for each channel cross-section. For the computation of suspended sediment, the median suspended grain diameter was obtained using:

$$\begin{aligned} d_{50,s}/d_{50} &= 1 + 0.011(\sigma_s - 1)(T_r - 25) \ \text{ for } \ 0 < T_r < 25 \\ d_{50,s}/d_{50} &= 1 \ \text{ for } \ T_r \geq 25 \end{aligned} \quad (1)$$

(van Rijn, 1984b), where $d_{50}$ is the median grain-size of the bed sediment, $\sigma_s$ is a sorting parameter given by $\sigma_s = 0.5(d_{84}/d_{50} + d_{50}/d_{16})$ and $T_r$ is a transport parameter defined here as $T_r = (\tau - \tau_{cr})/\tau_{cr}$, where $\tau$ is the time-averaged bed shear stress (see below) and $\tau_{cr}$ is the critical shear stress derived from the critical Shields $\theta_{cr} = \tau_{cr}g(\rho_s - \rho)d$, with $d = d_{50,s}$ for suspended and $d = d_{50}$ for bed load, $\rho_s$ and $\rho$ the grain and water density ($\rho_s = 2650$ kgm$^{-3}$ and $\rho = 1025$ kgm$^{-3}$ for seawater at 14 °C, salinity = 35 ppt, respectively) (Appendix 1).

### 3.2. Bed shear stress and bed roughness

ADV data were de-spiked and smoothed following standard procedures (Goring and Nikora, 2002). Zero-mean flow component time-series, $u'$, $v'$ and $w'$, comprised of a time-varying, turbulent component, and a more regular, semi-sinusoidal component, attributable to the oscillatory flows imposed on the tidal currents by waves. The first-order wave-induced time-series ($u_w$, $v_w$ and $w_w$) was effectively removed from the $u'$, $v'$ and $w'$ time-series using a moving average filter (Williams et al., 2003a) to leave turbulence-only flow components $u$, $v$ and $w$ The RMS wave-induced flow speed was calculated using $U_w = (\overline{u}_w^2 + \overline{v}_w^2)^{0.5}/\sqrt{2}$, where $\overline{u}_w$ and $\overline{v}_w$ are the wave variance values extracted from the PT time-series using a zero-crossing method combined with a Fast Fourier Transform (FFT) algorithm (Tucker and Pitt, 2001).

Time-averaged bed shear stress, used here to parameterise the combined forces of lift and drag that are primarily implicated with the mobilisation and transport of sediments, was calculated using the Turbulent Kinetic Energy (TKE) and Reynolds Stress (RS) methods (Williams et al., 2003a). In the TKE method, $\tau$ is defined as:

$$\tau_{\mathrm{TKE}}(z) = C\rho E(z) \quad (2)$$

(Soulsby and Humphery, 1990), where $C$ is a constant = 0.19 (Stapleton and Huntley, 1995), and the turbulent kinetic energy, $E$, at height $z$ is defined as $E(z) = 0.5(\overline{u}^2 + \overline{v}^2 + \overline{w}^2)$, where $\overline{u}$, $\overline{v}$ and $\overline{w}$ are the variance of the turbulence-only time-series. In the Reynolds stress method, $\tau$ is defined as:

$$\tau_{\mathrm{RS}}(z) = \rho\left(-\overline{uw}^2 + -\overline{vw}^2\right)^{0.5} \quad (3)$$

(Soulsby and Humphery, 1990) where $-\overline{uw}$ and $-\overline{ww}$ are the time-averaged Reynolds stresses. The time-averaged drag coefficient, $Cd$, at height $z$ above the bed was obtained using:

$$Cd(z) = (\overline{\tau}/\rho)/U_{DA}^2 \quad (4)$$

(Williams et al., 2003a) where $\overline{\tau}$ is the mean local bed shear stress defined as $(\tau_{TKE} + \tau_{RS})/2$ and $U_{\mathrm{DA}}$ the depth-averaged current velocity, approximated using the empirical equation (Soulsby, 1997):

$$U_{DA} = \overline{S}(z)/(z/0.32h)^{1/7} \quad (5)$$

with $\overline{S}(z) = (\overline{U}^2 + \overline{V}^2)^{1/2}$, where $\overline{U}$ and $\overline{V}$ denote time-averaged values of $U$ and $V$ at height $z$, and $h$ is the water depth.

The apparent bed roughness length, $z_a$, at height $z$ was estimated using:

$$z_a = z\exp^{-\left[\left(k/\sqrt{C_{d(z)}}\right)+1\right]} \quad (6)$$

where $k$ is the von Kármán constant (=0.4).

The total time-averaged shear stress, $\tau_0$, was also estimated using the simplified water slope method (Soulsby, 1997):

$$\tau_0 = \rho g\, hI \quad (7)$$

where $I$ is the water slope and $g$ acceleration due to gravity.

The validity of this approach was examined using the two dimensional hydro-morphodynamic numerical model XBeach (Roelvink et al., 2009). The model was set up using the measured bathymetry and topography of the Ancão Inlet and driven by the measured gradients in tidal elevation imposed on its seaward and lagoon boundaries. In addition, standard JONSWAP wave spectra were imposed on the seaward boundary of the model, with characteristics similar to those prevailing during the measurements (i.e. $H_s = 1$ m and $T_p = 6$ s). While most model parameters were set to commonly used values (Roelvink et al., 2009, Table 1), in this case the bed friction coefficient in the model ('*Cf*' in XBeach nomenclature) was adjusted until the depth-average current, $U_{\mathrm{DA}}$, predicted by the model at the ADV location in the Ancão Inlet matched closely the measured value (i.e. within 3%). This term is equivalent to a depth-averaged drag coefficient, $Cd_{\mathrm{DA}}$, and reflects the combined drag of sediment grains and bed forms. During the simulation period it was possible to match approximately predicted $U_{\mathrm{DA}}$ values with measured $U_{\mathrm{DA}}$ values using '*Cf*' = 0.005. However, in order to accurately simulate measured temporal changes in $U_{\mathrm{DA}}$ during the tidal cycle, multiple runs of XBeach were undertaken in which '*Cf*' was increased in incremental steps of 0.0002 between 0.002 and 0.015. The values of '*Cf*' providing the closest agreement between any given measured and simulated $U_{\mathrm{DA}}$ value were then identified.

Variability in bed form morphology is the result of a complex interaction between the bed, currents and unsteady shoaled waves of many frequencies and directions. In order to compute sediment transport it is necessary to quantify the drag of these bed forms to enable estimation of the skin-friction component of bed shear stress that drives sediment transport. Houwman and van Rijn (1999) have established a valuable relationship between the apparent bed roughness, $k_a = 30z_a$, and the physical bed roughness, $k_s = 30z_0$, in the form:

$$\frac{k_a}{k_s} = \exp(\gamma U_w/U_{DA}) \quad (8)$$

where $\gamma = 0.8 + \varphi - 0.3\varphi^2$, with $\varphi$ being the angle between wave and current direction (in radians). In the present study, estimates of $U_w$ were obtained from the ADV, $U_{\mathrm{DA}}$ and $k_a$ derived from Eqs. (5) and (6). Empirical relations between $k_a$ and $k_s$ were established for flood and ebb conditions. Here we only used ADV data with burst correlation coefficient values greater than 0.7. These empirical relationships express a wide range of situations, i.e., the

**Table 1**
XBeach parameter settings for Ancão Inlet.

| |
|---|
| **General constants** |
| rho = 1000 kgm$^{-3}$ (water density) |
| $g$ = 9.81 ms$^{-2}$ (acceleration of gravity) |
| **Wave input** |
| thetamin = −60 (lower directional limit) |
| thetamax = 60 (upper directional limit) |
| dtheta = 10 (directional resolution) |
| **Limiters** |
| CFL = 0.8 (maximum Courant number) |
| Eps = 0.1 (threshold depth for drying and flooding) |
| **Flow boundary conditions** |
| tideloc = 2 (number of input) |
| tidelen = 80 (length of tidal record) |
| paulrevere = 0 (option of sea/sea corner or sea/land corner specification) |
| front = 1 (seaward boundary conditions) |
| back = 2 (landward boundary conditions) |
| **Wave calculation options** |
| Hrms = 0 m (rms wave height) |
| wavint = 1000 s (interval between stationary wave module calls) |
| **Flow calculation options** |
| $C$ = 60 m$^{1/2}$s$^{-1}$ (Chezy coefficient) |
| **Time input for flow calculations** |
| tstart = 0 s (start time of simulation) |
| tint = 30 s (time interval output global values) |
| tstop = 14,220 s (stop time simulation) |
| **Sediment transport calculation options** |
| $d_{50}$ = 0.0088 m (grain diameter class of sediment) |
| $d_{90}$ = 0.0164 m (grain diameter class of sediment) |
| **Morphological calculation options** |
| morfac = 2.0 |
| **Output options** |
| zb (m, bed level) |
| dims ( |
| zs (m, water level) |
| H (m, wave height) |
| ue (ms$^{-1}$, Eulerian mean x-velocity cell centre) |
| ve (ms$^{-1}$, Eulerian mean y-velocity cell centre) |
| hh (m, water depth) |
| dzbdt (ms$^{-1}$, rate of change bed level) |
| sedero (m, cum. sedimention/erosion) |

instantaneous effect of wave-current interaction on the formation/destruction of bed forms through the tidal cycle.

### 3.3. Sediment transport

Estimates of the bed shear stress and apparent roughness were also obtained from the ADCP data. These data were rotated to align with the streamwise and spanwise directions and depth-averaged velocities were obtained for each 5 s velocity profile (or ensemble). The depth-averaged current velocity ($U_{DA}$) was obtained using:

$$U_{DA} = 1/h\int_0^h U(z)\mathrm{d}z \tag{9}$$

(Soulsby, 1997), where $U(z)$ is the current speed at height $z$ The von Kármán–Prandtl equation (Soulsby, 1997) was then used to obtain estimates of $\tau$ and $z_a$:

$$U(z) = \left(\sqrt{\tau/\rho}/k\right)\ln(z/z_0) \tag{10}$$

Using this relationship and following the linear regression of $U(z)$ on $ln(z)$, an apparent roughness is obtained by $z_a = \exp(-c/m)$, where $c$ is the intercept and $m$ is the slope. Using the above empirical relations between $k_a$ and $k_s$, an estimate of $z_0$ was obtained. Using Eq. (6), and replacing $z_0$ by $z_a$, the drag coefficient attributable to the bed forms is determined and then used to estimate the skin-friction component of shear stress, $\tau_s$, by Eq. (4). The skin-friction shields parameter ($\theta_s$) is then defined as:

$$\theta_s = \tau_s/g(\rho_s - \rho)d_{50} \tag{11}$$

For simplicity, other size fractions are not considered separately.

A unifying expression for the volumetric bed load transport rate (m$^2$s$^{-1}$), $q_b$, is given by:

$$q_b = \Phi\left[g(s-1)d^3\right]^{0.5} \tag{12}$$

(Soulsby, 1997), where $\Phi$ is the dimensionless bed load transport rate, with $d = d_{50}$. Here we apply four widely-used bed load formulae from Yalin (1964), van Rijn (1984a), Madsen (1991) and Nielsen (1992) to compute bed load transport rates for current-only conditions. These require estimates of the critical flow conditions necessary to initiate sediment transport. Both the bed load formulae and the methods used to estimate critical conditions are detailed in Appendix 1.

The volumetric suspended transport rate, $q_s$, was derived from:

$$q_s = \int_{za}^{h} C(z)U_{DA} \tag{13}$$

where $C(z)$ is the suspended sediment concentration at height $z$ and $za$ the reference concentration. The value of $C(z)$ was derived from three different methods, considering two methods for current-only processes, assuming a linear (power law, C-PL) or parabolic (Rouse profile, C-RP) increase of eddy diffusivity with depth, and one method for combined waves plus current situations (C-W). Using the ADV data, a statistically significant power law relationship between $q_s$ values obtained using different formulae and the parameter $U_{DA}d_{50,s}$ was obtained. The formulae used are detailed in Appendix 2 The method was first tested and validated at the Ancão Inlet and was then used to estimate $q_s$ across all the inlets using as input parameters the $U_{DA}$ values derived from the data collected with the ADCP and the sediment properties measured at each inlet (Table 2).

The resulting value of bed load, $q_b$, and suspended transport, $q_s$, computed using the above methods were used to define total transport, $q_t$, through a complete tidal cycle, under both spring- and neap tidal conditions. In the convention used here, negative and positive $q_t$ values are associated with ebb- and flood-tidal flow

**Table 2**
Summary of sediment parameters from analysis of samples and thresholds of motion derived from empirical formulae.

| | Ancão | Faro-Olhão | Armona | Fuseta | Tavira | Lacém |
|---|---|---|---|---|---|---|
| $d_{10}$ (mm) | 0.52 | 0.40 | 0.35 | 0.51 | 0.09 | 0.27 |
| $d_{16}$ (mm) | 0.59 | 0.46 | 0.41 | 0.59 | 0.21 | 0.31 |
| $d_{50}$ (mm) | 0.88 | 0.86 | 0.61 | 0.98 | 2.88 | 0.48 |
| $d_{84}$ (mm) | 1.38 | 5.19 | 1.08 | 2.10 | 6.29 | 0.81 |
| $d_{90}$ (mm) | 1.64 | 6.22 | 1.39 | 3.06 | 20.70 | 0.97 |
| *Carbonates (%)* | 5 | 17 | 6 | 6 | 24 | 6 |
| $\theta_{cr}$ | 0.029 | 0.029 | 0.031 | 0.030 | 0.042 | 0.033 |
| $\tau_{cr}$ (Nm$^{-2}$) | 0.421 | 0.410 | 0.302 | 0.468 | 1.933 | 0.256 |

General characteristics

| | |
|---|---|
| Ancão Inlet | Coarse sand, moderately well sorted; |
| Faro-Olhão Inlet | Varies from very coarse (margins less sorted) to medium sand (centre well sorted); |
| Armona Inlet | Coarse sand, moderately sorted; |
| Fuseta Inlet | Very coarse sand, general well sorted (less coarse and sorted at channel centre); |
| Tavira Inlet | Coarse sand (E margin) and fine gravel (W margin), both poorly sorted. At channel centre bedrock; |
| Lacém Inlet | Medium sand (margins) to coarse sand (channel centre), well sorted. |

directions, respectively. It should be borne in mind that $q_t$ values obtained in this study are only estimates and are site-specific.

### 3.4. Best estimates and measurement accuracy

Since field data are limited in space and time, it is difficult to make a direct comparison between the results presented in this paper and other studies on sediment transport. It is also complicated to perform statistical analysis to determine a range of conditions for the use of the given estimates, as well as it is to perform an error analysis. This is related to the inherent complexities of measuring sediment transport in the field, which makes the process of validating the applicability of empirical formulae on real field situations complex. van Rijn (2007a,b) combined several laboratory and field datasets to derive unified expressions of bed load and suspended transport under different grain-size diameters and coastal flow conditions (i.e. with combined quasi-steady tidal flow and surface waves). For bed load transport, van Rijn used the concept of instantaneous bed shear stress, the same as was used in the present study. The author also included the effect of variable bed roughness. Van Rijn pointed out the inherent difficulties of obtaining reliable field data on sediment transport on coastal conditions. To validate the bed load formulae for coastal flow, van Rijn (2007a) used a field dataset obtained by Hoekstra et al. (2001) with measured bed form migration rates. Overall, 80% of the predicted values are within a factor of 2 of the measured transport rates. For suspended sediment transport, several datasets on sediment concentration at different hydrodynamic conditions were used (see van Rijn, 2007b). The field data primarily showed that suspended transport in the coastal zone is strongly dependent on particle size and current velocity. Current-related suspended transport rates obtained by van Rijn (2007b) using van Rijn–Souls by equation (Eq. (13)) show reasonably good agreement (within a factor of 2 for measured values), for velocities in the range of 0.6–1.8 m/s.

Two of the only studies of sediment transport measurements at tidal inlets are the one performed by Williams et al. (2003a,b) at Ancão Inlet. Their study aimed to investigate the mean and turbulent flow fields, bed forms, and resuspension and transport of sediments, both suspended and bed load. Bed load transport calculated from measured bed form migration speeds and the measured suspended sediment flux agreed favourably with empirical predictions: $R^2 = 0.865$ to the mean of predicted values using various empirical formulae (van Rijn, 1984a; Madsen, 1991; Nielsen, 1992). Measured and predicted time-averaged sediment concentration profiles were found to be in close agreement with expressions for predicting current-only concentration profiles (Eq. (A6) power law, Appendix 2). An almost perfect match is attainable using slight adjustments to the shear stress or settling velocity values.

In the present study, the methodologies and techniques of Williams et al. (2003a,b) were followed to process the hydrodynamic variables. The method presented is considered to be the best estimate of both magnitude and trends of net sediment transport. Predicted bed load transport rates should range within a factor of 2 between measured and predicted values (e.g. based on ripple migration rates and empirical bed load transport equations, respectively), while a close match between measured and predicted concentration profiles is expected (e.g. measured concentration profiles derived by an acoustic backscatter system/pump samples and theoretic profiles by Eq. A6 and A7 equations, Appendix 2, respectively). Although care must be taken on extrapolating the results to evaluate the long-term behaviour of tidal inlet function and evolution, the methodology can be used to evaluate inlet flushing capacity under fair-weather condition and contributes to expand knowledge on inlet dynamics and provide useful data for numerical modelling of sediment transport in a tidal inlet system.

## 4. Results

### 4.1. Bed shear stress and bed roughness

Fig. 2A shows temporal changes and a clear time lag between water levels measured by the PTs over a period of ~5 h Fig. 2B shows temporal changes in the total shear stress obtained by the simplified water slope method (Eq. (7)) and the time-average shear stress values (Eq. (2) and (3)) derived from the ADV. Time-averaged (~1 s) values of $U_{DA}$ and $U_w$ are shown in Fig. 2C and D, while $\overline{\tau}$ values are shown in Fig. 2E and their components in Fig. 2F. Maximum values of $U_{DA}$ $O$ (1.2 $ms^{-1}$) were measured during flood and ebb tides at the ADV location, over the range 0.10 m < h < and 2.22 m. Wave-induced flow speeds averaged $U_w$ $O$(0.25 $ms^{-1}$), increasing to $U_w$ $O$(0.35 $ms^{-1}$), around flood peak.

Although showing the same general trends and magnitudes, TKE-derived values of $\overline{\tau}$ are always slightly higher than RS-derived values (Fig. 2), and have a lower variance. Both the RS and TKE methods fail to provide meaningful estimates of bed shear stress at the early stages of the ebb tide. It is thought that this result reflects boundary interference as a bed form migrated beneath the ADV and prevented the instrument from working. Current induced shear stress is the main component of the mixed tide/wave dominated flow in the inlet, with instantaneous values in the range 0.7 $Nm^{-2}$–4.9 $Nm^{-2}$ (Fig. 2F). This is approximately the same range of values as the mean current-wave instantaneous shear-stresses. Although waves induce generally lower instantaneous shear-stresses (0.3 $Nm^{-2}$–1.1 $Nm^{-2}$), maximum instantaneous shear stress values computed for combined current–wave processes, using the wave boundary layer model (Fredsøe, 1984), were actually higher (2.2 $Nm^{-2}$ and 6.5 $Nm^{-2}$).

Strong tidal currents $\overline{S}_{max}$ $O$(1.9 $ms^{-1}$) in the Ancão Inlet resulted in the formation of a sequence of relatively long-crested bed forms, similar to megaripples, with their crests aligned approximately normal to the mean tidal flow direction (Fig. 3A). Small current-wave generated ripples also formed, their length related to near-bed orbital velocity. In order to examine the links between measured bed roughness and bed morphology, two different empirical equations were used to estimate ripples (Nielsen, 1992; van Rijn, 1993). These gave a mean ripple wavelength $O(\lambda_r = 1.22$ m) and heights $O(\Delta_r = 0.23$ m: Fig. 3B and C). These values are similar to the dimensions of the megaripples measured in the field $O(\lambda_r = 1.7$ m and $\Delta_r = 0.16$ m). Owing to the coarse nature of bed sediments, and their instability with the flow, small ripples superimposed on megaripples were not predicted by the empirical formulae.

Values of $k_a$ and $k_s$ are shown on Fig. 4, where $k_s$ values were determined based on two linear relationships for flood/ebb conditions derived from Eq. (8) (Fig. 4A). The ratio between $k_a/k_s$ ranges between 1.1 and 2.0, with a mean value of 1.4. Results indicate that $U_w$ does not contribute significantly to mean $U_{DA}$ (i.e. the ratio $U_w/U_{DA}$ ranges between 0.07 and 0.83 $ms^{-1}$, with a mean value of 0.34 $ms^{-1}$). Time-averaged $k_s$ were found to be *c.* 0.088 m and thus similar to values measured in other studies over rough, mobile sediment beds (e.g. up to 0.1 m, van Rijn, 2007a). However, maximum $k_s$ values of 0.23 m were obtained during peak flood tide flows and are probably related to dune-like features (Fig. 4B). Computed values for $k_a$ range from 0.006 m to 0.426 m, with a mean value of $O$(0.13 m) during the tidal cycle. Similar results are reported by Houwman and van Rijn (1999), who show that $k_a$ is an almost constant value of 0.1 m $U_w$ in the range 0.3–1.5 $ms^{-1}$.

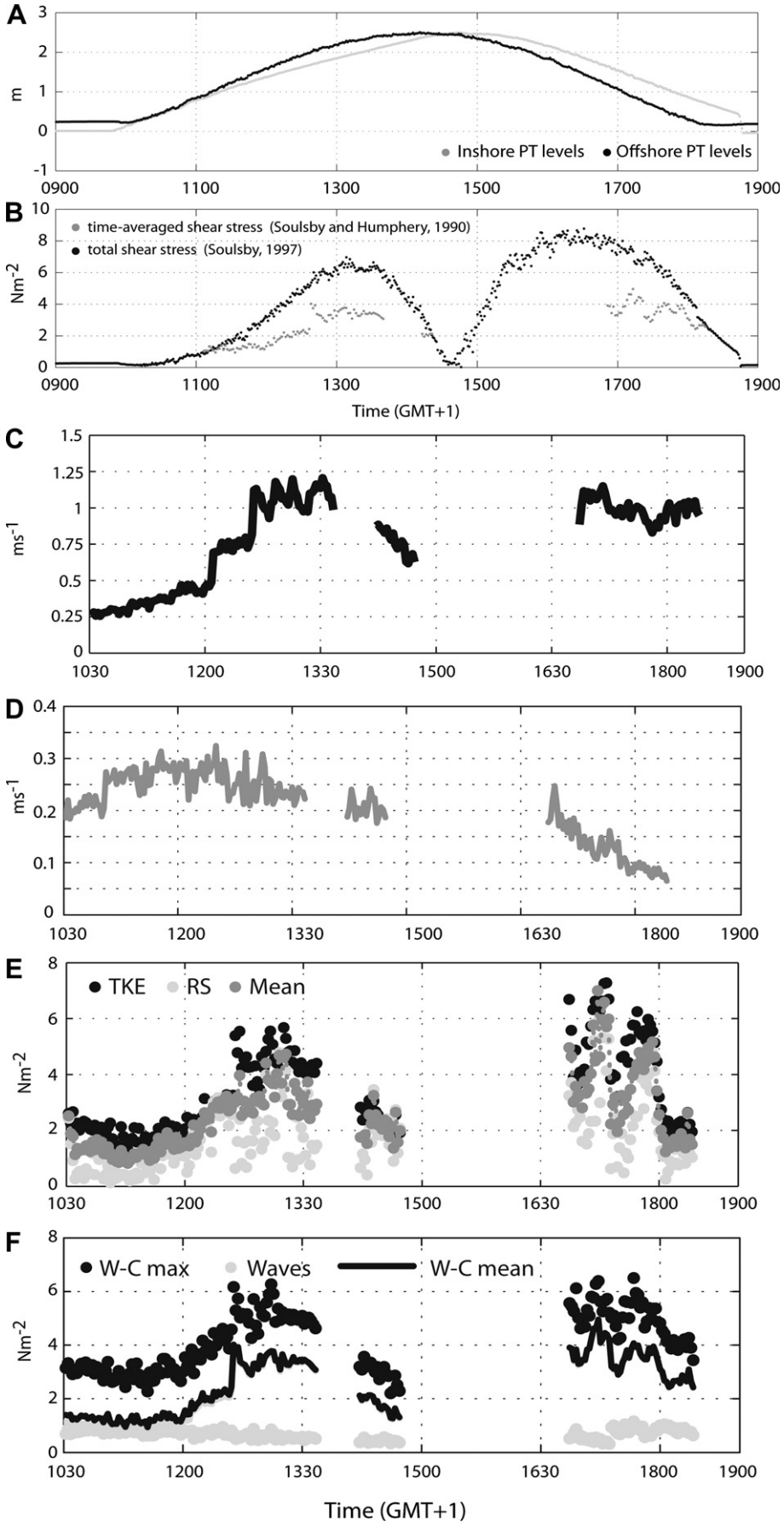


**Fig. 2.** Offshore/inshore pressure transducer levels (A); $\tau_0$ (water slope method) and $\tau$ (mean of RS and TKE methods) (B); 1 s burst average values of $U_{DA}$ (C); $U_w$ (D); $\tau_{TKE}$ and $\tau_{RS}$ (E); and $\tau$ components (F).

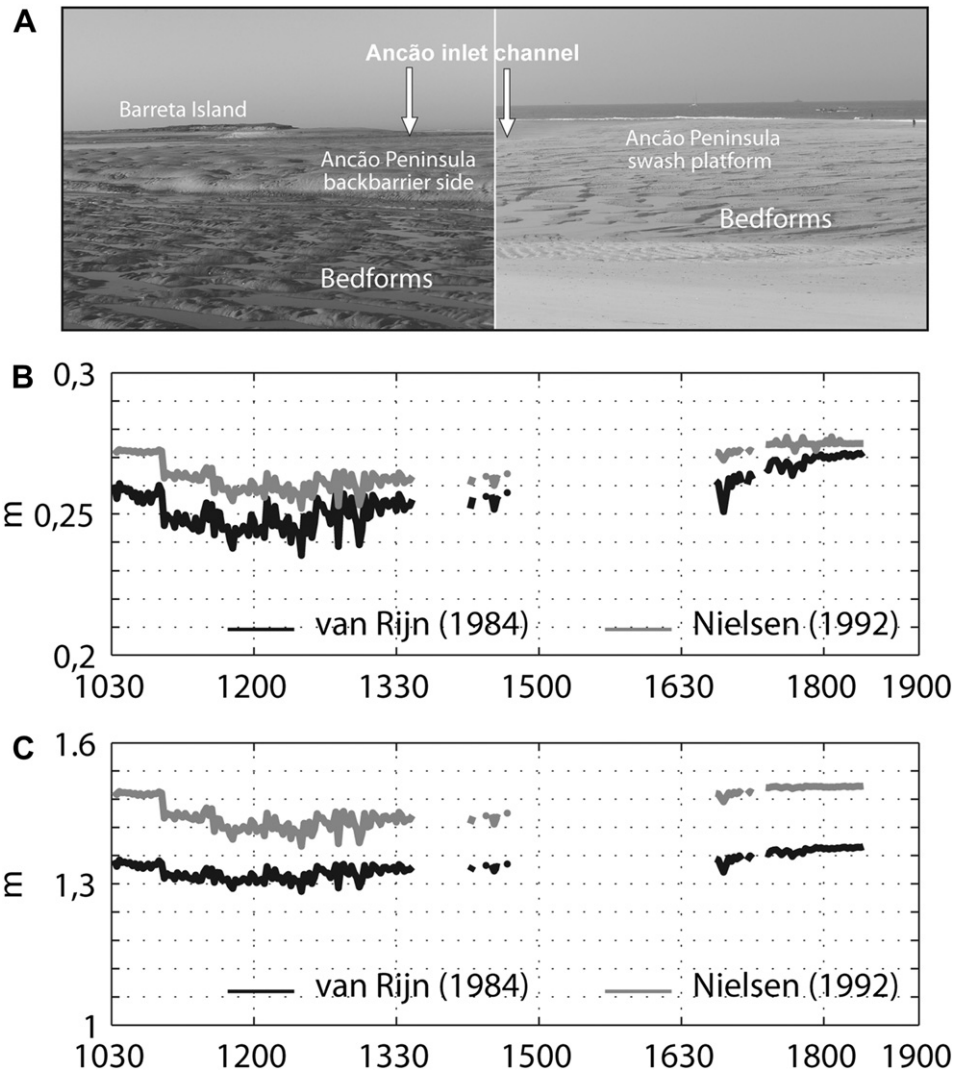


**Fig. 3.** Bedforms morphology at the inner inlet channel, backbarrier side and at the updrift swash platform, Ancão Peninsula (A); height (A) and length (B) of bedforms determined empirically (van Rijn, 1984c; Nielsen, 1992).

Estimates of *Cd* obtained from Eq. (4) range between 0.005 and 0.015, with maximum values in the initial stages of the flood (Fig. 4C). Those values can be compared with '*Cf*' values obtained from XBeach (Fig. 4D). Although '*Cf*' values are slightly higher, they reveal the same tendency, thus providing strong evidence that the water slope method gives a good estimate of total drag.

### 4.2. Sediment transport – the Ancão Inlet test case and its application

Samples of surficial bed sediments collected across the inlet cross-section using a grab had the following grain-size characteristics: $d_{10} = 0.52$ mm, $d_{16} = 0.59$ mm, $d_{50} = 0.88$ mm, $d_{84} = 1.38$ mm and $d_{90} = 1.64$ mm (i.e. coarse sand). Suspended sediment grain-size was determined empirically using Eq. (1). Theoretical threshold values of shear stress, $\tau_{cr}$, and Shields parameter, $\theta_{cr}$, were determined using the formulae detailed in Appendix 1, summarised in Table 2.

The suspended sediment transport rate was obtained by multiplying the depth-averaged velocity by the mean suspended sediment concentration predicted by power law expressions (Fig. 5). Analysing the coefficients obtained, it can be observed that $q_s$ correlates best with $\overline{U}d_{50s}$ to the power of ~4. This is in agreement with other studies (e.g. Dyer, 1986). Peak values of suspended transport were $O(0.028\ \mathrm{kgm^{-1}s^{-1}})$ during the peak flood in combined current-wave situations. Generally, average values for current-only and current-wave interaction lay between 0.01 and 0.015 $\mathrm{kgm^{-1}s^{-1}}$, slightly higher during the flood tide and insensitive to the computation method.

Predicted net bed load and suspended transport produced by different methods are given in Fig. 6, along with total net sediment transport rates for a spring-tidal cycle in Ancão Inlet. During the early stages of flood/ebb tide and when the tide falls to slack water, $q_b$ <0.25 $\mathrm{kgm^{-1}s^{-1}}$ (Fig. 6B), which is coincident with $U_{DA}$ <0.6 $\mathrm{ms^{-1}}$ (Fig. 6A). When that velocity is exceeded, $q_b$ increases to values between 0.25 and 0.5 $\mathrm{kgm^{-1}s^{-1}}$, with maxima >0.75 $\mathrm{kgm^{-1}s^{-1}}$ coincident with $U_{DA}$ >1.5 $\mathrm{ms^{-1}}$. Values of $q_s$ have the same tendency (Fig. 6C), although at a lower magnitude (approximately 10% of bed load transport rates), i.e., when $U_{DA} > 0.6\ \mathrm{ms^{-1}}$, $q_s$ range between 0.025 and 0.05 $\mathrm{kgm^{-1}s^{-1}}$, with maxima >0.075 $\mathrm{kgm^{-1}s^{-1}}$ when $U_{DA} > 1.5\ \mathrm{ms^{-1}}$.

Integrated values of $q_b$ and $q_s$ through the tidal cycle are presented in Table 3, with net sediment transport rates obtained by the mean of the values given by different methods. The $q_b$ methods differ by a maximum factor of 2, with van Rijn (1984a) method producing higher estimates. The value of $\overline{q_b}_{Ebb}$ is approximately three times higher than $\overline{q_b}_{Flood}$, resulting in $\overline{q_b}_{Net} \sim -0.084 \pm 0.03\ \mathrm{kgm^{-1}s^{-1}}$, i.e.,

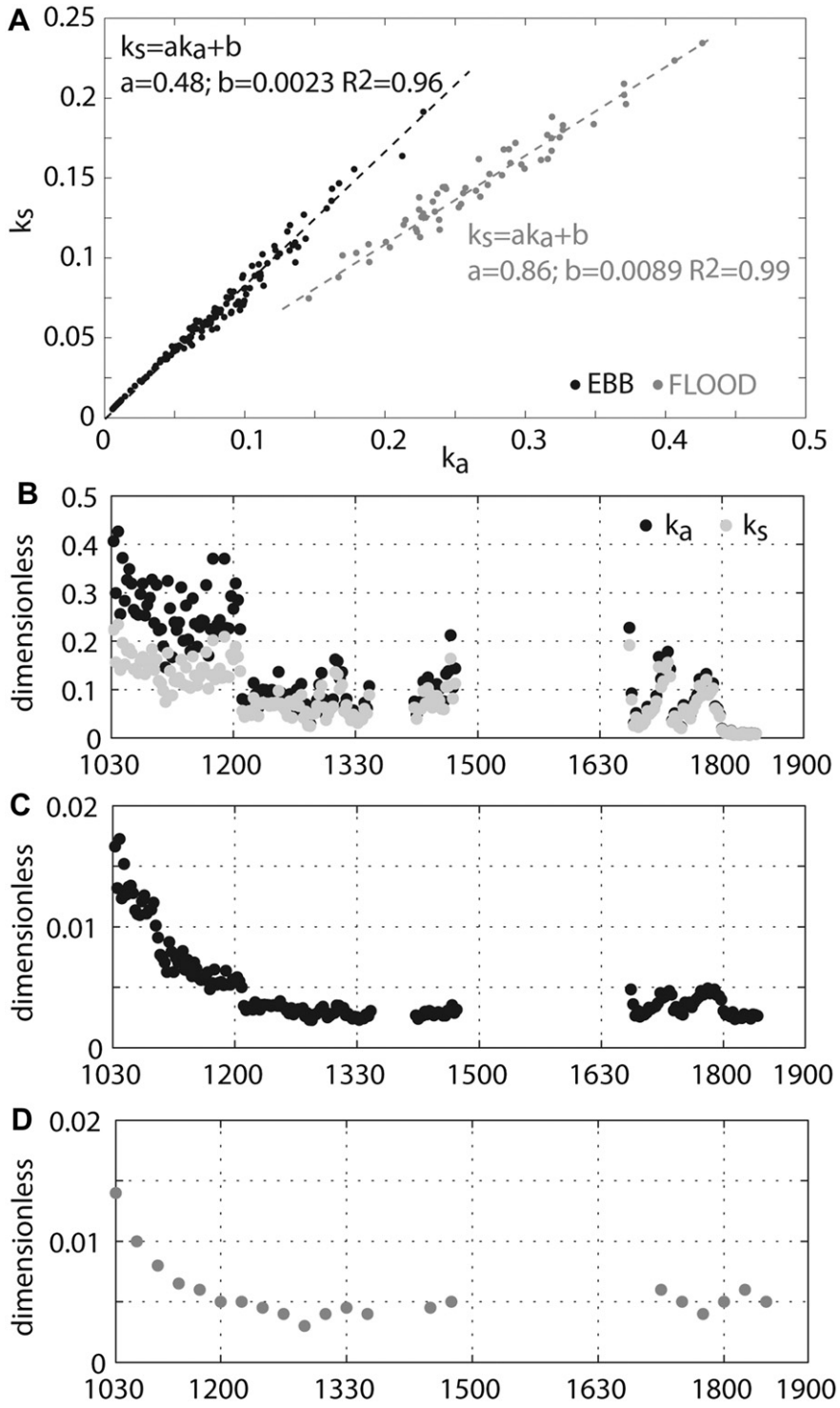


**Fig. 4.** Flood/ebb derived relations between $k_a$ and $k_s$ from Eq. (8) (A); 1 s burst average values $k_a$ and $k_s$ values (B); *Cd* (C); and *Cf* mean values determined by the XBeach (D).

net sediment export. Current-only and current-wave methods to derive $q_s$ provide approximate values, resulting in $\overline{q_s}_{Net}$ $-0.011 \pm 0.001$ kgm$^{-1}$s$^{-1}$, i.e. also net sediment export.

### 4.3. Net sediment transport estimates through Ria Formosa inlets

The same methodology, primarily validated for the spring-tide ADCP survey at Ancão Inlet, was then applied to the other inlets, for both spring and neap tidal cycles. Table 4 presents the volumetric transport rates (spring and neap measurements) for the Ria Formosa inlets, which are assumed to represent the volumetric transport occurring under fair-weather conditions. The grain-size properties of surficial bed sediment samples across each transect are presented in Table 2. All the inlet channels contain medium-to-coarse sand, poorly sorted in the adjacent channels. With the exception of Tavira Inlet, more than 80% of the sediment is composed of terrigenous material (almost entirely quartz), the remaining fraction being shell fragments. Entrainment thresholds,

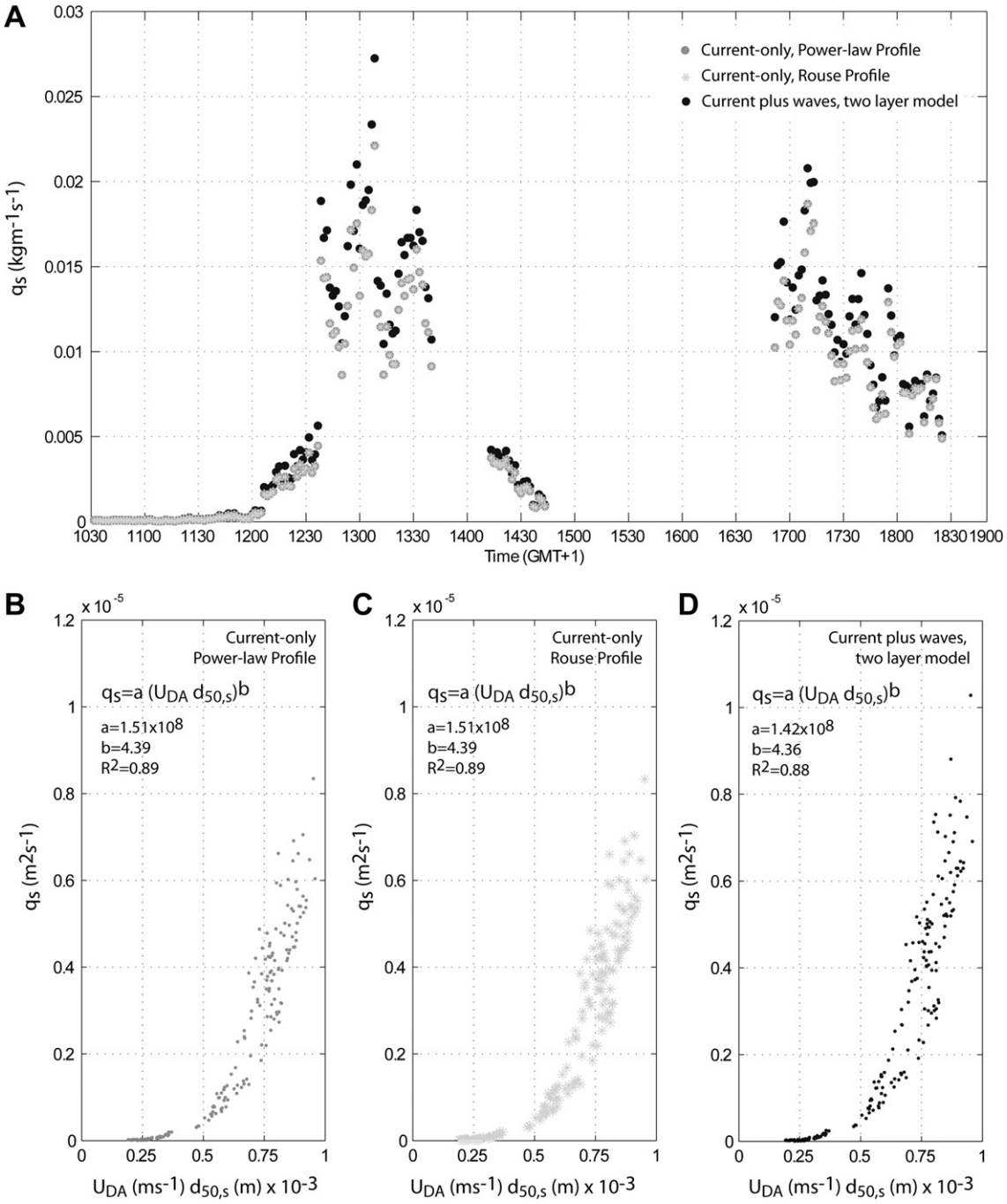


**Fig. 5.** Mass suspended sediment rate thought the tidal cycle at Ancão inlet (A) and volumetric transport rate as a function of the depth-average velocity for current-only processes with eddy diffusivity varying linearly; parabolically (B) with the flow; and for the current-wave interaction (C).

expressed as a critical Shields parameter and as a critical bed shear stress, are also presented in Table 2.

At Ancão Inlet, net sediment transport estimates revealed that the ebb currents are capable of flushing out sediments that enter the inlet during the flood tide under both spring and neap tide conditions (Table 4). Application of the method to the Faro-Olhão Inlet, the main inlet of the system (Fig. 8), results in onshore net transport (Table 4) under both spring and neap tide conditions. The inlet is flood dominated, presenting a flood prism consistently higher than the ebb prism (Salles et al., 2005; Pacheco et al., 2010). The inlet acts as a net importer to the system, which confirms the numerical simulation on net sediment transport performed by Salles et al. (2005) and agrees with the annual net volumes of accretion/erosion obtained in Faro Channel, comparing pre- and post-dredging surveys at the site (Pacheco et al., 2008). Net sediment transport estimates for Armona Inlet (Table 4) confirm the prevalence of offshore net transport during fair-weather conditions. Ebb currents seem to be capable of flushing sediments offshore, a characteristic enhanced during spring-tides. Fuseta Inlet (Fig. 9A and B) also presents net sediment export (Table 4). The inlet was artificially opened in 1999 and the relocation process was considered to be less successful than that of Ancão Inlet (Vila-Concejo et al., 2004b), perhaps related to the lack of space to accommodate the flood delta. The persistence of the opening is

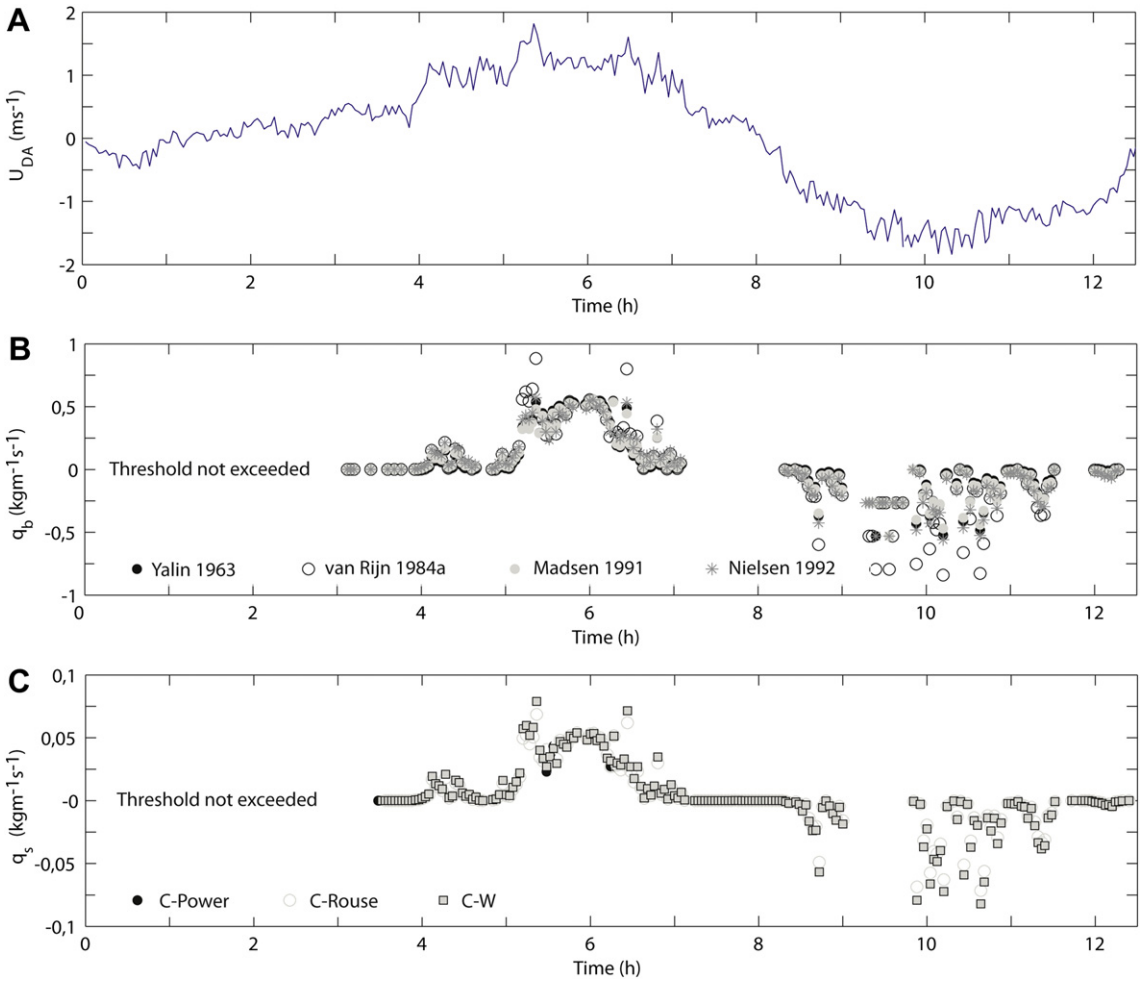


**Fig. 6.** Interpolated values of $U_{DA}$ (A), $q_b$ (B) and $q_s$ (C) derived from the ADCP and sediment properties data for the spring-tide tidal cycle survey performed at Ancão tidal inlet.

clear evidence of the inlet's flushing capacity. At Tavira Inlet (Fig. 10AA and B), the combination of flow and sediment properties resulted in an overall net transport rate of zero (Table 4). The sediments in the inlet channel of Tavira Inlet are very coarse (Table 2), thus less mobile, and thresholds of motion were never exceeded. As a result, sediment exchange through the inlet is negligible in both directions, indicating an overall equilibrium between hydraulics and the bed. Finally, Lacém Inlet (Fig. 10A–C) presents net import during spring-tides and negligible export during neap tides (Table 4). As shown at Fuseta Inlet, backbarrier space to accommodate the flood delta is limited, but in contrast to Fuseta Inlet, the inlet is always flood dominated (Vila-Concejo et al., 2006; Pacheco et al., 2010). The inlet typically develops an updrift SW oriented swash bar. When SW waves act with the flood currents on the updrift swash bar, variable amounts of sediment are transported landward, constricting the inlet channel and eventually leading to inlet closure (Fig. 10C).

## 5. Discussion

This study shows that both measured rates of bed load and suspended transport are in accordance (magnitude and direction) with the results obtained by Williams et al. (2003a,b). Rates of bedload transport derived from measured bed form migration rates in Ancão Inlet by Williams et al. (2003a) range between 0.2 kgm$^{-1}$s$^{-1}$ and 0.4 kgm$^{-1}$s$^{-1}$ (cf. Fig. 6B); while acoustic measurements of suspended sediment transport rates obtained by the same authors ranged between 0.01 kgm$^{-1}$s$^{-1}$ and 0.02 kgm$^{-1}$s$^{-1}$ and were essentially time-invariant (cf. Fig. 5A). Results obtained by Williams et al. (2003a,b) were found to correlate linearly ($R^2 = 0.865$) to the mean of predicted values using various empirical formulae (van Rijn, 1984a; Madsen, 1991; Nielsen, 1992), the same used in the present study. The empirical methods used by Williams et al. (2003a) to calculate bed load differed by

**Table 3**
Estimates of mass (kgm$^{-1}$s$^{-1}$) and volumetric (m$^3$year$^{-1}$) transport rates using different models for bed load and suspended transport for a ADCP tidal cycle performed at Ancão inlet during spring-tides.

| Bed load transport | Flood (kg/m/s) | Ebb (kg/m/s) | Net (kg/m/s) |
|---|---|---|---|
| Yalin (1964) | 0.046 | −0.114 | −0.068 |
| van Rijn (1984a,b,c) | 0.071 | −0.195 | −0.124 |
| Madsen (1991) | 0.050 | −0.115 | −0.065 |
| Nielsen (1992) | 0.066 | −0.144 | −0.078 |
| *Mean* | *0.058* | *−0.142* | *−0.084* |
| *Standard deviation* | *0.012* | *0.038* | *0.027* |
| Suspended transport | | | |
| C-Rouse () | 0.006 | −0.017 | −0.010 |
| C-Power () | 0.006 | −0.017 | −0.010 |
| C-W () | 0.007 | −0.019 | −0.012 |
| *Mean* | *0.007* | *−0.018* | *−0.011* |
| *Standard deviation* | *0.001* | *0.002* | *0.001* |

**Table 4**
Estimates of mass ($kgm^{-1}s^{-1}$) transport rates using an average of the different models for bed load and suspended transport for spring/neap ADCP tidal cycles for the inlets of the the Ria Formosa; the maximum velocity ($U_{cs}$) and residual tidal prism ($P$) directions (adapted from Pacheco et al., 2010).

| Inlet | Description | Parameter | Tide condition | |
|---|---|---|---|---|
| | | | Spring-tide | Neap tide |
| Ancão | Relocated inlet (1997) and let to evolve naturally; cyclic eastward migration | $q_b$ (kg/m/s) | −8.350E−02 | −2.98E−04 |
| | | $q_s$ (kg/m/s) | −1.100E−02 | −4.50E−05 |
| | | $q_t$ (kg/m/s) | −9.45E−02 | −3.43E−04 |
| | | $U_{cs}$ maximum[a] | Ebb directed | Ebb directed |
| | | *Residual P*[a] | Ebb directed | Ebb directed |
| Faro-Olhão | Artificially open and stabilised (dual jetty) (open year 1929–1957) | $q_b$ (kg/m/s) | 1.05E−02 | 8.56E−06 |
| | | $q_s$ (kg/m/s) | 7.85E−07 | 3.24E−08 |
| | | $q_t$ (kg/m/s) | 1.05E−02 | 8.59E−06 |
| | | $U_{cs}$ maximum[a] | Flood directed | Flood directed |
| | | *Residual P*[†] | Flood directed | Flood directed |
| Armona | Natural inlet; location stable through recent centuries; narrowing and losing hydraulic efficiency since Faro-Olhão opening | $q_b$ (kg/m/s) | −2.47E−03 | 2.58E−03 |
| | | $q_s$ (kg/m/s) | −1.61E−05 | 6.12E−05 |
| | | $q_t$ (kg/m/s) | −2.49E−03 | 2.64E−03 |
| | | $U_{cs}$ maximum[a] | Ebb directed | Ebb directed |
| | | *Residual P*[†] | Ebb directed | Ebb directed |
| Fuseta | Relocated inlet (1999) and let to evolve naturally; cyclic eastward migration | $q_b$ (kg/m/s) | −1.53E−02 | −2.13E−02 |
| | | $q_s$ (kg/m/s) | −1.55E−03 | −1.92E−04 |
| | | $q_t$ (kg/m/s) | −1.69E−02 | −2.15E−02 |
| | | $U_{cs}$ maximum[a] | Flood directed | Flood directed |
| | | *Residual P*[†] | Flood directed | Flood directed |
| Tavira | Artificially open (1927) and stabilised (dual jetty) | $q_b$ (kg/m/s) | 0.00E + 00 | 0.00E + 00 |
| | | $q_s$ (kg/m/s) | 0.00E + 00 | 0.00E + 00 |
| | | $q_t$ (kg/m/s) | 0.00E + 00 | 0.00E + 00 |
| | | $U_{cs}$ maximum[a] | Ebb directed | Ebb directed |
| | | *Residual P*[†] | Ebb directed | Ebb directed |
| Lacém | Natural inlet; cyclic eastward migration | $q_b$ (kg/m/s) | 6.49E−04 | −2.87E−02 |
| | | $q_s$ (kg/m/s) | −3.83E−05 | −3.85E−04 |
| | | $q_t$ (kg/m/s) | 6.11E−04 | −2.91E−02 |
| | | $U_{cs}$ maximum[a] | Flood directed | Ebb directed |
| | | *Residual P*[†] | No residual | Ebb directed |

a maximum factor of 3, while for the present study the maximum derivation between methods was 2. This last can be related to more calm wave conditions.

The proportion of total sediment transport in the Ancão Inlet composed of suspended material was ~10% of bed load transport, while for Williams et al. (2003a) measurements was ~30%. This discrepancy also indicates that the contribution of the wave–current interaction on sediment resuspension events was lower, which seems to be confirmed by the close match between current-only and current–wave estimates (Table 3). Both studies indicate that $q_s$ is limited by the availability of fine sediment in the relatively coarse and well sorted bed sediments of Ancão Inlet. The migrating megaripples and dune-like bed features observed at most locations in the inlet are responsible for the majority of bed load transport. Despite the presence of waves, the bulk of suspended sediment transport is accomplished by turbulent diffusion processes related to the strong tidal currents (cf. Williams et al., 2003a). Also, the bed form dimensions in the inlet scale with the grain-size and confirm with theoretical predictions for ripples. The height and length of the megaripples derived from various empirical formulae (Fig. 3, van Rijn, 1984c; Nielsen, 1992) are in accordance with the results obtained by Williams et al. (2003a,b).

Measured maximum values of shear stress ($\tau_s$) at Ancão Inlet, recorded at ebb stage during spring-tides and under fair-weather conditions, are close to the upper limit of shear stress for inlet stability (~5 $Nm^{-2}$, Fig. 2E, F) defined by Bruun and Gerritsen (1959) and Bruun (1978). Those studies argue that inlet stability is governed by shear stress along the channel bottom. Our study showed that changes in hydraulic bed roughness between flood and ebb tides, as result of current velocity induced changes to bed morphology, tended to enhance sediment transport offshore (Figs. 2F and 6).

Approximately, 13 years after relocation, the Ancão Inlet maintains its capacity to flush sediments while continuing to migrate.

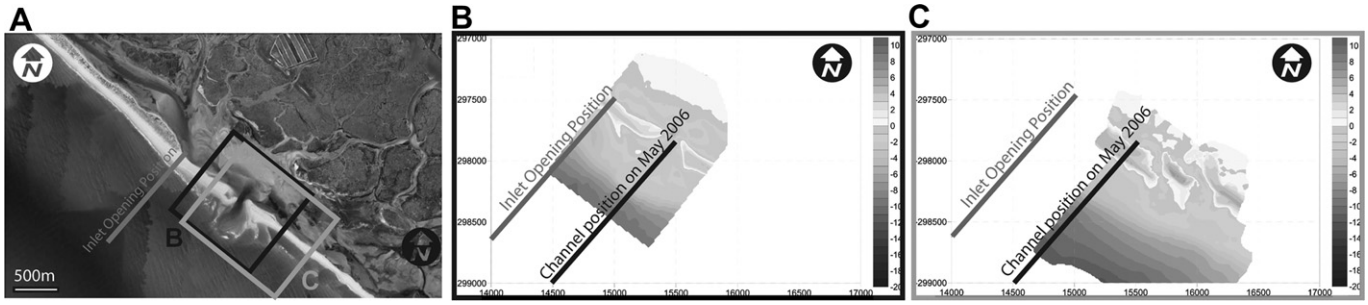


**Fig. 7.** (A) Ancão Inlet in 2006, showing the inlet opening position (1997); (B) the limits of the topo-bathymetric survey performed during the ADCP measurements; and (C) the limits of the topo-bathymetric survey (April 2010) performed after the storm of March 2010, with the new inlet position (eastward inlet) leading to the closure of the former one.

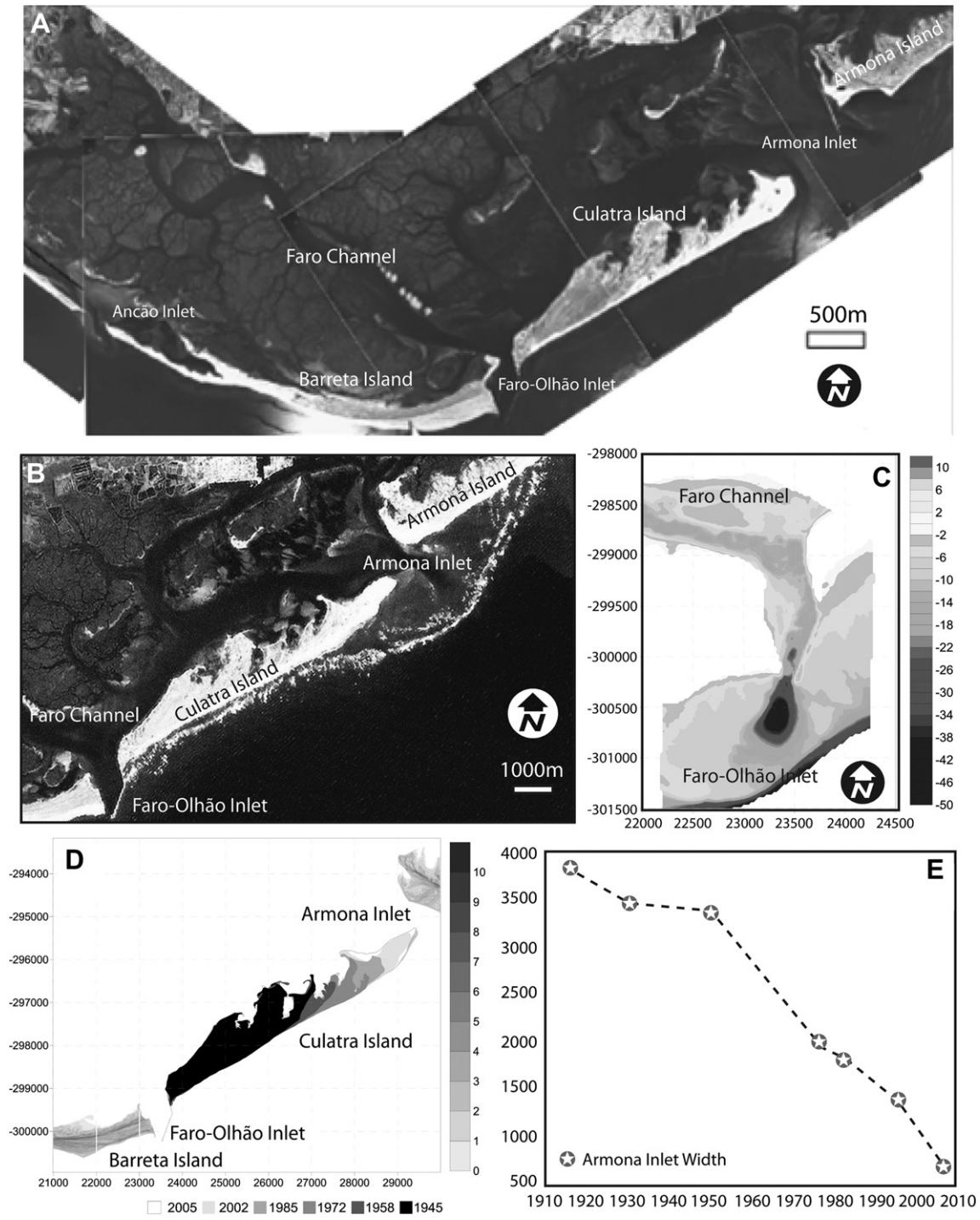


**Fig. 8.** (A) Western sector inlets in 1976 and (B) 2006, the latter showing the Armona ebb-delta terminal lobe; (C) Faro-Olhão Inlet survey (2006), showing the actual maximum depth (~50 m) and offshore extension of the scouring process; (D) Culatra Island evolution, after the completion of opening and stabilisation works at Faro-Olhão Inlet and (E) the simultaneous narrowing of Armona Inlet.

The inlet, since its opening in 1997, has migrated ~1100 m (~86 m/year, last measurement on April, 2010, Fig. 7) and has maintained its ebb-dominance (Williams et al., 2003c; Vila-Concejo et al., 2004b; Salles et al., 2005; Pacheco et al., 2010), except during periods of increased wave activity when the inlet becomes wave dominated (Morris et al., 2001, 2004). Ebb-dominance enhances the inlet's flushing capacity and is an important factor contributing to the success of inlet relocation (Vila-Concejo et al., 2004a).

Estimates of sediment transport collected under prevailing fair-weather conditions can be used on reporting system flushing capacity, an important factor on maintaining multiple inlets open. The net sediment transport estimates correlate directly with the values of maximum cross-sectional velocity, directions and residuals measured by both Salles et al. (2005) and Pacheco et al. (2010), using different datasets and methods (numerical modelling vs. field-based studies): net export of sediments at Ancão, Armona,

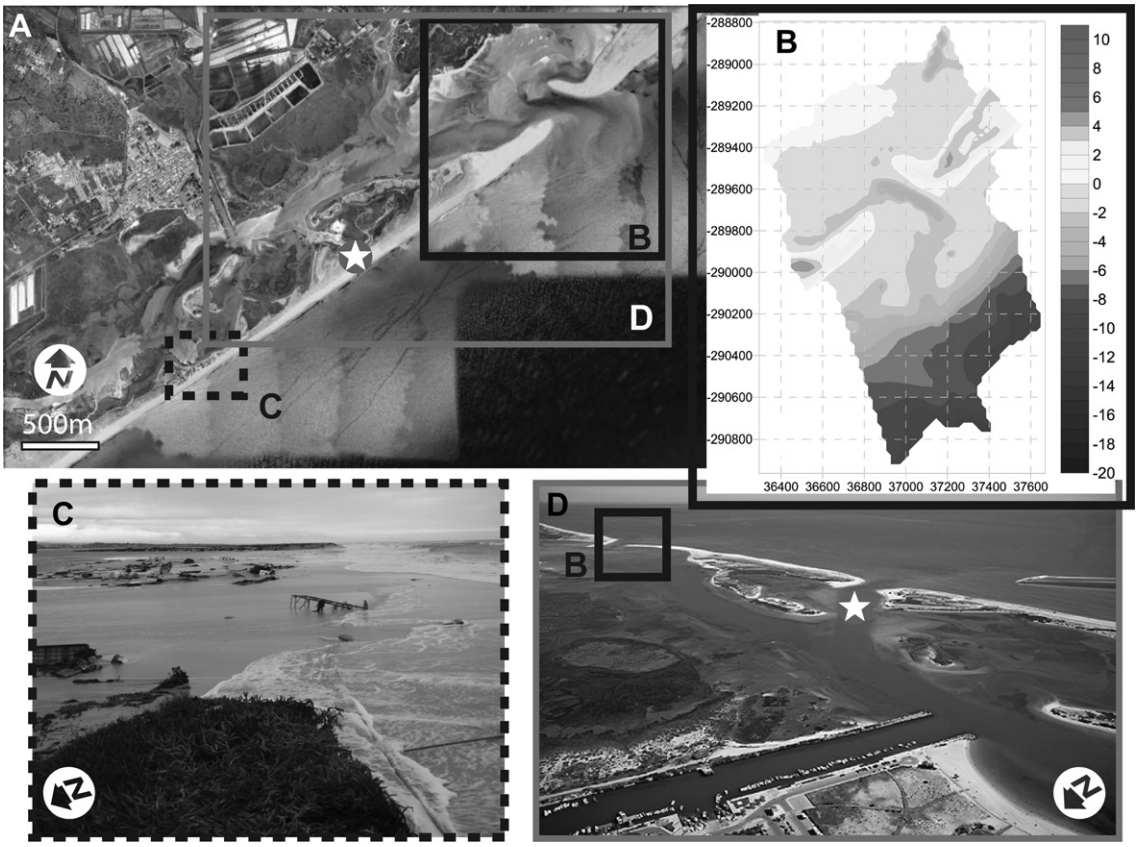


**Fig. 9.** (A) Fuseta Inlet at the time of the ADCP measurements (2006), showing the topo-bathymetric survey limits performed in May 2006; (B) the breaching at the "Natural Inlet Location" resulting from a storm on 2nd March 2010; (C) artificial closure of the new inlet breach and (D) the new artificial relocation (indicated by a star); still the old inlet (measured in this study) remained open and was later closed artificially by coastal authorities.

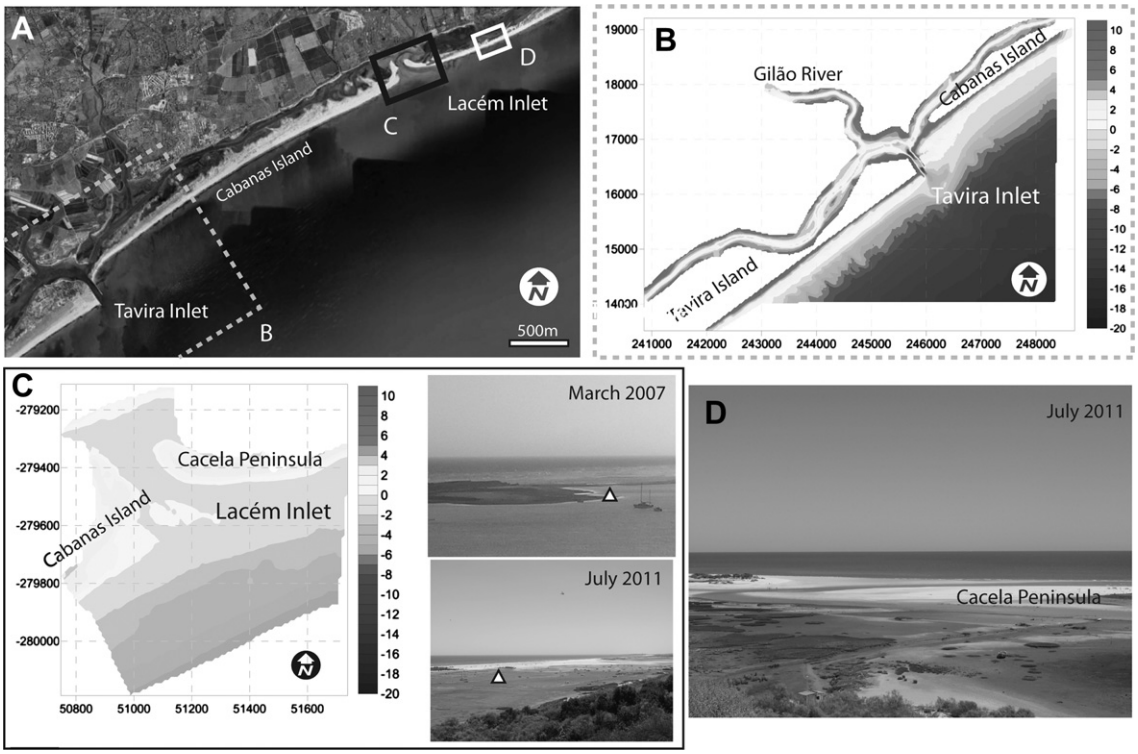


**Fig. 10.** (A) Aerial photography showing both Tavira and Lacém inlets (2006); bathymetric surveys of the (B) Tavira and (C) Lacém inlets performed in May 2007, the latter showing complementary oblique photos of the SW updrift-oriented swash bar that eventually led to inlet closure (the arrow indicates the inlet opening location); (D) the new artificial relocation performed in summer 2010.

Fuseta and Tavira; net import at Faro-Olhão and Lacém inlets (Table 4). These findings demonstrate the utility of maximum velocity ($U_{cs}$) and residual tidal prism ($P$) direction as indicators of prevailing net sediment transport. As pointed out by van de van de Kreeke and Robaczewska (1993; see also Salles et al., 2005), it is the existence of residual flows between the inlets, together with the direction of the maximum velocity, that ultimately determines the flow (Pacheco et al., 2010) and transport dominance (this study) in a given inlet, superceding the effects of tidal distortion.

Episodic events, such as storms, can open natural inlets through the system and recent observations clearly report the system's ability to maintain those inlets open through periods of variable length. This happened recently at the relocated inlets Ancão and Fuseta. At the first site forced a migration by jump, with a natural closure of the westward inlet and persistence of the new inlet (Fig. 7); at the second site, a westward opening in a more natural and favourable position (according to Vila-Concejo et al., 2002, 2006), which provoked a series of engineering interventions in the system (Fig. 9).

During storm events, or when increased wave activity is combined with flood currents, the inlets can import significant quantities of sand to the flood deltas. The amount imported is thought to depend on the availability of sand offshore (i.e. on ebb shoals and by littoral drift). Despite the inlets' known capacity to redeposit sediments offshore under fair-weather conditions, net sediment influx can reduce the hydraulic efficiency of the channels. An example of this occurred at the natural Armona Inlet, an inlet with a stable location and persistency since the XVI century. This inlet was formerly the main inlet of the Ria Formosa (Fig. 8), before the opening and stabilisation westward of Faro-Olhão Inlet. Hydrodynamic measurements has showed that Armona Inlet is ebb dominated under spring/neap tide conditions and is always hydrodynamically connected with Faro-Olhão Inlet throughout the lunar tidal cycle (Pacheco et al., 2010) This interconnection enhances its flushing capacity, especially during spring-tides. However, following Faro-Olhão Inlet opening, Armona Inlet has been gradually losing its hydraulic efficiency, resulting in a large reduction in its cross-sectional area (Fig. 8D, E). The collapsed ebb-tidal delta (Pacheco, in press) is contributing sediment to the narrowing Armona Inlet (Fig. 8E) and to expansion of Culatra Island (Fig. 8D). Ebb-tidal delta volumetric changes, related to coastline adjustments to recent engineering actions (Gau and Collins, 1994; Elias and van der Spek, 2006; Pacheco et al., 2008), are the factors that ultimately control multi-inlet system stability. The Armona Inlet case highlights the importance that ebb-tidal deltas have in trapping longshore-transported sediment and releasing it again during periods of increased wave activity.

The global tidal prism distribution at Ria Formosa (Pacheco et al., 2010), as in other multi-inlet systems worldwide, changes considerably between spring and neap tides. Residual flow between inlets can play an important role in enhancing stability, as can the morphology of the inner channels connecting inlets (van de Kreeke et al., 2008). Although the evolution of cross-sectional area is a valuable parameter for assessing inlet stability (Escoffier, 1977), and which has been extended to analyse multiple inlet stability (van de Kreeke, 1990), it should be complemented by analysing other variables. A full evaluation of the stability of multiple inlet systems requires a detailed coupling of nonlinear dynamics (Salles et al., 2005), with quantification of net sediment transport and its relation with hydrodynamic patterns through the inlet cross-section (Pacheco et al., 2010; this study). It also should include the effect of waves over the ebb-tidal delta, especially their role in stirring and transporting the sediment under increase periods of wave activity. The present methodology to derive net sediment transport estimated under fair-weather conditions can be effectively used to compute medium- to long-term sediment budgets and predict inlet evolution, if coupled with a rational statistic quantification of similar net transport estimates under episodic storm events. The latter requires further research.

## 6. Summary and conclusion

Field-based studies of sediment transport have the potential to quantify the magnitude and direction of net sediment transport and may assist in identifying evolutionary trends for a single or multiple inlet system. The capacity of an inlet to flush sediments during prevailing fair-weather conditions is not sufficient to counter the entry of sediment during periods of storm activity or under intense wave/current interaction. Although the largest morphological changes occur during storm events, the day-to-day interception of longshore-transported sand, and its passage through and past an inlet, is governed by fair-weather hydrodynamics, and these processes were measured and modelled in this work. Existing data on the Ria Formosa, both past and present, confirm the utility of estimates of fair-weather sediment transport on reporting system flushing capacity. This is an important factor for maintaining multiple inlets open. The sediment transport estimates presented in this study accurately reproduce the magnitude and direction of sediment transport and correlate directly with the residuals and maximum velocity and direction of the flow measured at the site. These findings favour the use of the mean depth-average cross-sectional velocity along a tidal cycle and residual tidal prism as a criterion to evaluate inlets' capacity to flush sediments offshore, with implications for the analysis of equilibrium in single- and multi-inlet systems. The approach appears to be robust and widely applicable. It can therefore be applied under the same conditions at any tidal inlet system and may be of particular importance when attempting to understand sediment transport at inlet mouths, quantify infilling rates and define optimal dredging volumes.

## Acknowledgements

This work is a contribution to the IDEM project – Inlet Dynamics Evolution and Management at the Ria Formosa, under contract POCI/MAR/56533/2004. André Pacheco and Erwan Garel were supported by Fundação para a Ciência e a Tecnologia, grant numbers SFRH/BD/28257/2006 and SFRH/BPD/34475/2006. We gratefully acknowledge everyone at CIACOMAR who participated in data collection, as well as skippers Marinho, Janaca and Esmeraldo. We are especially grateful to Luis Pedro Almeida and Jamie Mitchell for their valuable assistance in surveying and to Simon Connor for his English correction and constructive criticism to early versions of this manuscript. We would also like to thank the anonymous reviewers for their suggestions that substantially improved the paper.

## Appendix 1. Estimation of critical flow conditions and bed load sediment transport

The critical Shields parameter, $\theta_{cr}$, is defined as:

$$\theta_{cr} = \frac{0.30}{1 + 1.2D_*} + 0.055[1 - \exp(-0.020D_*)] \quad \text{(A1)}$$

(Soulsby, 1997), with $D_* = (g(s-1)/\upsilon^2)^{1/3} d_{50}$, where $s$ is the ratio of densities of grain and water (2.58) $g$ is acceleration due to gravity ($=9.81\ \mathrm{m^2 s^{-1}}$) and $\upsilon$ is the kinematic viscosity of water ($=1.36 \times 10^{-6}\ \mathrm{m^2 s^{-1}}$).

The four bed load formulae used in the present study take the form:

(1) Yalin (1964)

$$\Phi = F_Y\theta_s^{0.5}(\theta_s-\theta_{cr}), F_Y = 0.635/\theta_{cr}[1-(1/aT)\ln(1+aT)] \quad \text{(A2)}$$

with $a = 2.45\theta_{cr}^{0.5}s^{-0.4}$ and $T = (\theta_s-\theta_{cr})/\theta_{cr}$

(2) van Rijn (1984a)

$$\Phi = F_R\theta_s^{0.5}\left(\theta_s^{0.5}-\theta_{cr}^{0.5}\right)^{2.4},\ F_R = \left(0.005/Cd^{1.7}\right)(d/h)^{0.2} \quad \text{(A3)}$$

(3) Madsen (1991)

$$\Phi = F_M(\theta_s-0.7\theta_{cr})(\theta_s-\theta_{cr}),\ F_M = 8/\tan\ \phi_i \quad \text{(A4)}$$

where $\phi_i$ is the angle of grain repose in degrees.

(4) Nielsen (1992)

$$\Phi = 12\theta_s(\theta_s-\theta_{cr}) \quad \text{(A5)}$$

## Appendix 2. Estimation of suspended sediment transport

Two equations used here to describe the vertical profile of suspended sediment, *C-Profile*, for current-only situations take a power law:

$$C(z) = C_a(z/za)^{-b} \quad \text{(A6)}$$

and a parabolic (Rouse profile)

$$C(z) = C_a((z/za)(h-za/h-z))^{-b} \quad \text{(A7)}$$

form, where $C(z)$ is the suspended sediment concentration at height $z$, $C_a$ is the reference concentration at height $za$, the exponent $b$ is the Rouse number given by $b = w_s/(ku_*)$, where $u_* = (\tau_s/\rho)^{0.5}$. Values for $C_a$ were obtained by taking the average of three different estimates of $C_a$ from Smith and McLean (1977), van Rijn (1984b) and Zyserman and Fredsøe (1994). For natural sands the settling velocity is given by:

$$w_s = (\nu/d)\left[\left(10.36^2+1.049D_*^3\right)^{0.5}-10.36\right] \quad \text{(A8)}$$

(Soulsby, 1997)

For combined waves plus currents situations the *C-Profile* was calculated using:

$$C(z) = C_a\left(\frac{z}{za}\right)^{-b\ \max} \quad \text{for } za \le z \le z_w \quad \text{(A9)}$$

$$C(z) = C(z_w)\left(\frac{z}{za}\right)^{-bm} \quad \text{for } z_w < z \le h \quad \text{(A10)}$$

Soulsby (1997), where $z_w$ is the wave boundary thickness, $z_w = (u_{*\max}T_s)/2\pi$, $u_{*\max}$ is the maximum bed friction velocity, $T_s$ is the peak wave period, $b_{max}$ and $b_m$ are the maximum and minimum Rouse numbers given by $b_{\max} = w_s/ku_{*\max}$ and $b_m = w_s/ku_{*m}$, where $u_{*m}$ is the mean bed friction velocity. The values of $u_{*m}$ and $u_{*\max}$ are given by $u_{*m} = (\tau_m/\rho)^{0.5}$ and $u_{*\max} = (\tau_{\max}/\rho)^{0.5}$, with $\tau_{max}$ and $\tau_m$ as the maximum and mean bed shear stress in a wave cycle. The values of $\tau_{max}$ and $\tau_m$ were obtained from the ADV data, through the use of the analytical wave-current boundary layer model proposed by Fredsøe (1984).

## References


Bishop, C.T., Donelan, M.A., 1987. Measuring waves with pressure transducers. Coastal Eng 11, 309–328.

Blott, S.J., Pye, K., 2001. GRADISTAT: a grain size distribution and statistics package for the analysis of unconsolidated sediments. Earth Surf. Process. Landf. 26, 1237–1248.

Bruun, P., Gerritsen, F., 1959. Natural bypassing of sand at coastal inlets. J. of the Waterways and Harbors Div. 85, 75–107.

Bruun, P., 1978. Stability of tidal inlets, theory and engineering. Dev. Geotech. Eng. 23, 510.

Costa, M., Silva, R., Vitorino, J., 2001. Contribuição para o estudo do clima de agitação marítima na costa Portuguesa. 2as Jornadas Portuguesas de Engenharia Costeira e Portuária CD-ROM (in Portuguese).

Dyer, K.R., 1986. Coastal and Estuarine Sediment Dynamics. Wiley-Interscience, New York. 342pp.

Elias, E.P.L., van der Spek, A.J.F., 2006. Long-term morphodynamic evolution of Texel Inlet and its ebb-tidal inlet (The Netherlands). Mar. Geol. 225, 5–21.

Escoffier, F.F., 1977. Hydraulics and stability of tidal inlets. General investigation of tidal inlets (GITI) Report 13, U.S. Army Engineer Waterway Experiment Station, Vicksburg, MS, 72 pp.

FitzGerald, D.M., 1996. Geomorphic variability and morphologic and sedimentologic controls on tidal inlets. J. Coast. Res. SI 23, 47–71.

FitzGerald, D.M., Kraus, N.C., Hands, E.B., 2001. Natural Mechanisms of Sediment Bypassing at Tidal Inlets. ERDC/CHL CHETN-IV-30. U.S. Army Engineer Research and Development Center, Vicksburg, MS. 10pp.

Folk, R.L., Ward, W.C., 1957. Brazos River bar: a study in significance of grain size parameters. J. Sediment. Petrol 27, 3–26.

Fredsøe, J., 1984. Turbulent boundary layer in wave-current motion. J. Hydraul. Eng. ASCE 110, 1103–1120.

Gao, S., Collins, M., 1994. Tidal inlet equilibrium, in relation to cross-sectional area and sediment transport patterns. Estuar. Coast. Shelf Sci. 38, 157–172.

Goring, D.G., Nikora, V.I., 2002. Despiking acoustic Doppler velocimeter data. J. Hydraul. Eng 128 (1), 117–126.

Hayes, M.O., 1979. Barrier island morphology as a function of tidal and wave regime. In: Leatherman, S.P. (Ed.), Barrier Islands: From the Gulf of St. Lawrence to the Gulf of Mexico. Academic Press, New York, N.Y, pp. 1–27.

Hoekstra, P., Bell, P., Van Santen, P., Roode, N., 2001. Intertidal bedforms and bedload transport measurements on Spratt Sand, Teignmouth (UK). Coastal Dynamics, Lund, Sweden, pp. 1028–1037.

Houwman, K.T., van Rijn, L.C., 1999. Flow resistance in the coastal zone. Coastal Eng. 38, 261–273.

Kana, T.W., Stevens, F.D., 1992. Coastal geomorphology and sand budgets applied to beach nourishment. Proc. Coastal Engineering Practice '92, ASCE, VA, 29–44.

Kana, T.W., Hayter, E.J., Work, P.A., 1999. Mesoscale sediment transport at southeastern U.S. tidal inlets: conceptual model applicable to mixed energy settings. J. Coast. Res. 15 (2), 303–313.

Madsen, O.S., 1991. Mechanics of cohesionless sediment transport in coastal waters. Proc. Coastal Sediments, ASCE, 15–27.

Morris, B.D., Davidson, M.A., Huntley, D.A., 2001. Measurements of the response of a coastal inlet using video monitoring techniques. Mar. Geol. 175, 251–272.

Morris, B.D., Davidson, M.A., Huntley, D.A., 2004. Estimates of the seasonal morphological evolution of the Barra Nova inlet using video techniques. Cont. Shelf. Res. 24, 263–278.

Nielsen, I., 1992. Advanced Series on Ocean Engineering. Coastal Bottom Boundary Layers and Sediment Transport, vol. 4. World Scientific Publishing, Singapore.

Oertel, G.F., 1972. Sediment transport on estuary entrance shoals and the formation of swash platforms. J. Sediment. Petrol 42, 858–868.

Pacheco, A., Vila-Concejo, A., Ferreira, Ó, Dias, J.A., 2008. Assessment of tidal inlet evolution and stability using sediment budget computations and hydraulic parameter analysis. Mar. Geol. 247, 104–127.

Pacheco, A., Ferreira, Ó, Williams, J.J., Garel, E., Vila-Concejo, A., Dias, J.A., 2010. Hydrodynamics and evolution of a multiple-inlet system. Mar. Geol. 274, 32–42.

Pacheco, A., Ferreira, Ó., Williams, J.J., in press. Long-term morphological impacts of the opening of a new inlet on a multiple inlet system. Earth Surf. Process. Landf. doi:10.1002/esp.2193.

Roelvink, J.A., Reniers, A., van Dongeren, A., de Vries, J., McCall, R., Lescinski, J., 2009. Modeling storm impacts on beaches, dunes and barrier islands. Coastal Eng. 56 (11–12), 1133–1152.

Rosati, J.D., Kraus, N.C., 1999. Formulation of sediment budgets at inlets. Coast. Eng. Tech., 20. Note IV-15.

Rosati, J.D., 2005. Concepts in sediment budgets. J. Coast. Res. 21 (2), 307–322.

Salles, P., Voulgaris, G., Aubrey, D., 2005. Contribution of nonlinear mechanisms in the persistence of multiple tidal inlet systems. Estuar. Coast. Shelf. Sci. 65, 475–491.

Smith, J.D., McLean, S.R., 1977. Spatially averaged flow over a wavy surface. J. Geophys. Res. 82 (12), 1735–1746.

Soulsby, R.L., 1997. Dynamics of marine sands. A manual for practical applications. HR Wallingford Report SR 466, 142 pp.
Soulsby, R.L., Humphery, J.D., 1990. Field observations of wave-current interaction at the sea bed. In: Tørum, A., Gudmestad, O.T. (Eds.), Water Wave Kinematics. Kluwer Academic Publishers, Dordrecht, pp. 413–428.
Stapleton, R.L., Huntley, D.A., 1995. Seabed stress determination using the inertia dissipation method and turbulent kinetic energy method. Earth Surf. Process. Landf. 20, 807–815.
Tucker, M.J., Pitt, E.G., 2001. Waves in Ocean Engineering. Elsevier Ocean Engineering Book Series, vol 5. Elsevier, Amsterdam. 521.
van de Kreeke, J., 1990. Multiple tidal inlets be stable? Estuar. Coast. Shelf Sci. 30, 261–273.
van de Kreeke, J., Robaczewska, K., 1993. Tide-induced residual transport of coarse sediment; application to the ems estuary. Netherland, J. of Sea Res. 31 (3), 209–220.
van de Kreeke, J., Brouwer, R.L., Zitman, T.J., Schuttelaars, H.M., 2008. The effect of a topography high on the morphological stability of a two-inlet bay system. Coast. Eng. 55, 319–332.
van Rijn, L.C., 1984a. Sediment transport, Part I: bed load transport. J. Hydraul. Eng. 110 (11), 1431–1456.
van Rijn, L.C., 1984b. Sediment transport, Part II: suspended load transport. J. Hydraul. Eng. 110 (11), 1613–1641.
van Rijn, L.C., 1984c. Sediment transport, Part III: bed forms and alluvial roughness. J. Hydraul. Eng. 110 (12), 1733–1754.
van Rijn, L.C., 1993. Principles of Sediment Transport in Rivers, Estuaries and Coastal Seas. Aqua Publications, Amsterdam. 614pp.
van Rijn, L.C., 2007a. United view of sediment transport by currents and waves I: initiation of motion, bed roughness and bed load transport. J. Hydraul. Eng, ASCE 133 (6), 649–667.
van Rijn, L.C., 2007b. United view of sediment transport by currents and waves II: suspended transport. J. Hydraul. Eng, ASCE 133 (6), 668–689.
Vila-Concejo, A., Matias, A., Ferreira, Ó., Duarte, C., Dias, J.M.A., 2002. Recent evolution of natural inlets of a barrier island system in southern Portugal. J. Coast. Res. (Special issue 36), 741–752.
Vila-Concejo, A., Ferreira, Ó, Matias, A., Morris, B.D., Dias, J.A., 2004a. Lessons from inlet relocation: examples from Southern Portugal. Coast. Eng. 51 (10), 967–990.
Vila-Concejo, A., Ferreira, Ó, Ciavola, P., Matias, A., Dias, J.A., 2004b. Tracer studies on the updrift margin of a complex inlet system. Mar. Geol. 208, 43–72.
Vila-Concejo, A., Matias, A., Pacheco, A., Ferreira, Ó, Dias, J.M.A., 2006. Inlet hazard determination in the Ria Formosa barrier island system. Cont. Shelf. Res. 26 (9), 1045–1060.
Williams, J.J., Bell, P.S., Thorne, P.D., 2003a. Field measurements of flow fields and sediment transport above mobile beds. J. Geophy. Res. 108 (C4), 3109.
Williams, J.J., Bell, P.S., Humphery, P.J., Hardcastle, P.J., Thorne, P.D., 2003b. New approach to measurement of sediment processes in a tidal inlet. Cont. Shelf. Res. 23, 1239–1254.
Williams, J.J., O'Connor, B.A.O., Arens, S.M., Abadie, S., Bell, P., Balouin, Y., Van Boxel, J.H., do Carmo, A.J., Davidson, M., Ferreira, Ó, Heron, M., Howa, H., Hughes, Z., Kaczmarec, L.M., Kim, H., Morris, B., Nicholson, J., Pan, S., Salles, P., Silva, A., Smith, J., Soares, C., Vila-Concejo, A., 2003c. Tidal inlet function: field evidence and numerical simulation in the INDIA project. J. Coast. Res. 19 (1), 189–211.
Yalin, M.S., 1964. Geometrical properties of sand waves. J. Hydraul. Div., Proc. ASCE 90 (HY5), 105–119.
Zyserman, J.A., Fredsøe, J., 1994. Data analysis of bed concentration of sediment. J. Hydraul. Eng. ASCE 120 (9), 1021–1042.